Supplement of The Cryosphere, 19, 1181–1203, 2025
https://doi.org/10.5194/tc-19-1181-2025-supplement

The Cryosphere Open Access EGU

Supplement of

Bathymetry-constrained impact of relative sea-level change on basal melting in Antarctica

Moritz Kreuzer et al.

Correspondence to: Moritz Kreuzer (kreuzer@pik-potsdam.de)

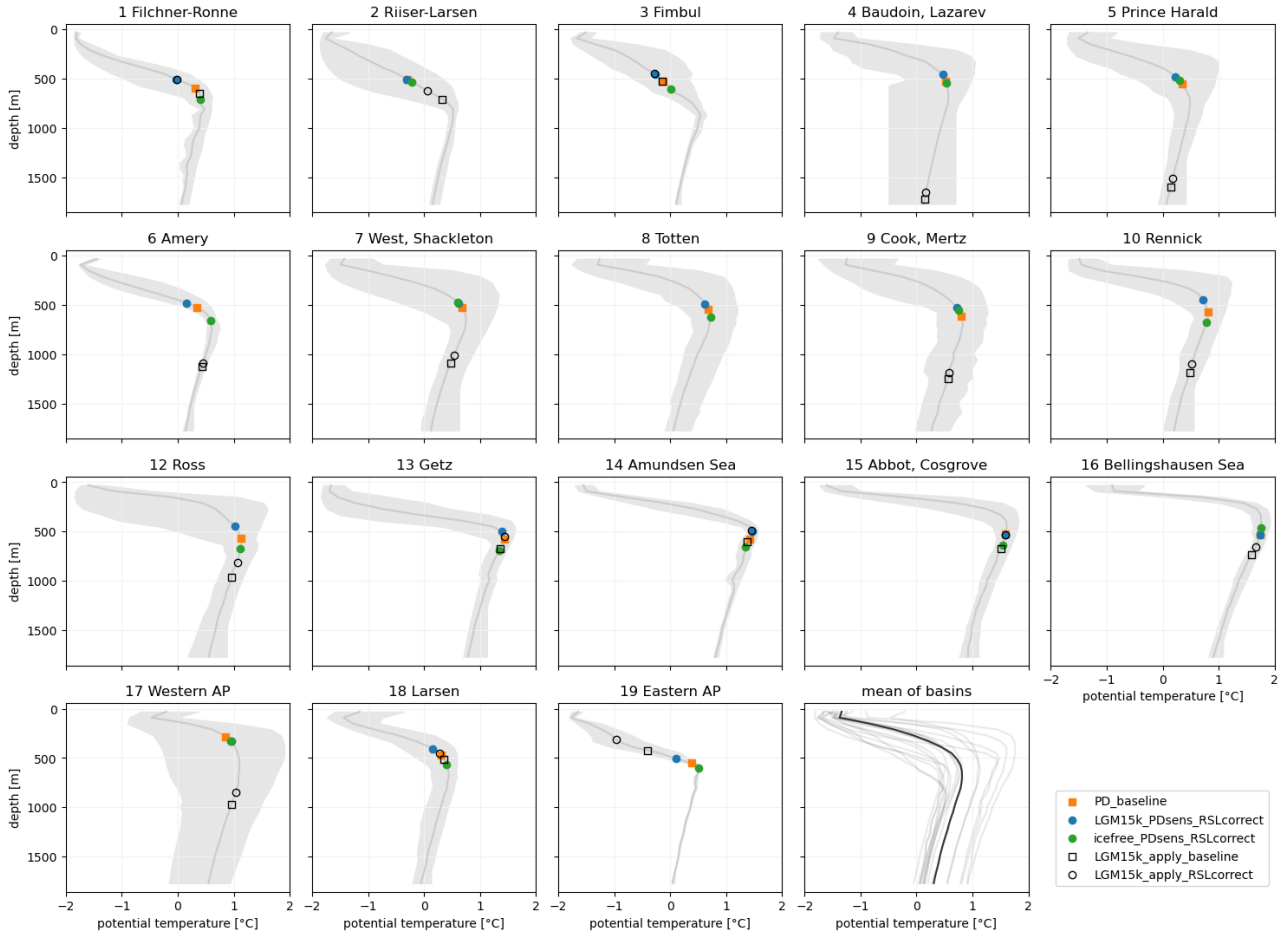

Figure S1. Vertical temperature profiles at continental-shelf break mask. Solid line shows basin mean profile, while shaded area marks the spread between minimum and maximum values. Basin numbers and names are displayed for each subplot. Points on the mean profile indicate the grounding line access depth $d_{\mathrm{GL},0}$ for experiments using *LGM15k* and *icefree* RSL configurations. The rightmost subplot in the last row shows each basin mean profile with light gray lines and the mean over the circumpolar continental shelf break in black color. Continental-shelf break is defined along the 1800 m isobath surrounding the Antarctic Ice Sheet, with a width of 40 km. Data used from Jourdain et al. (2020).

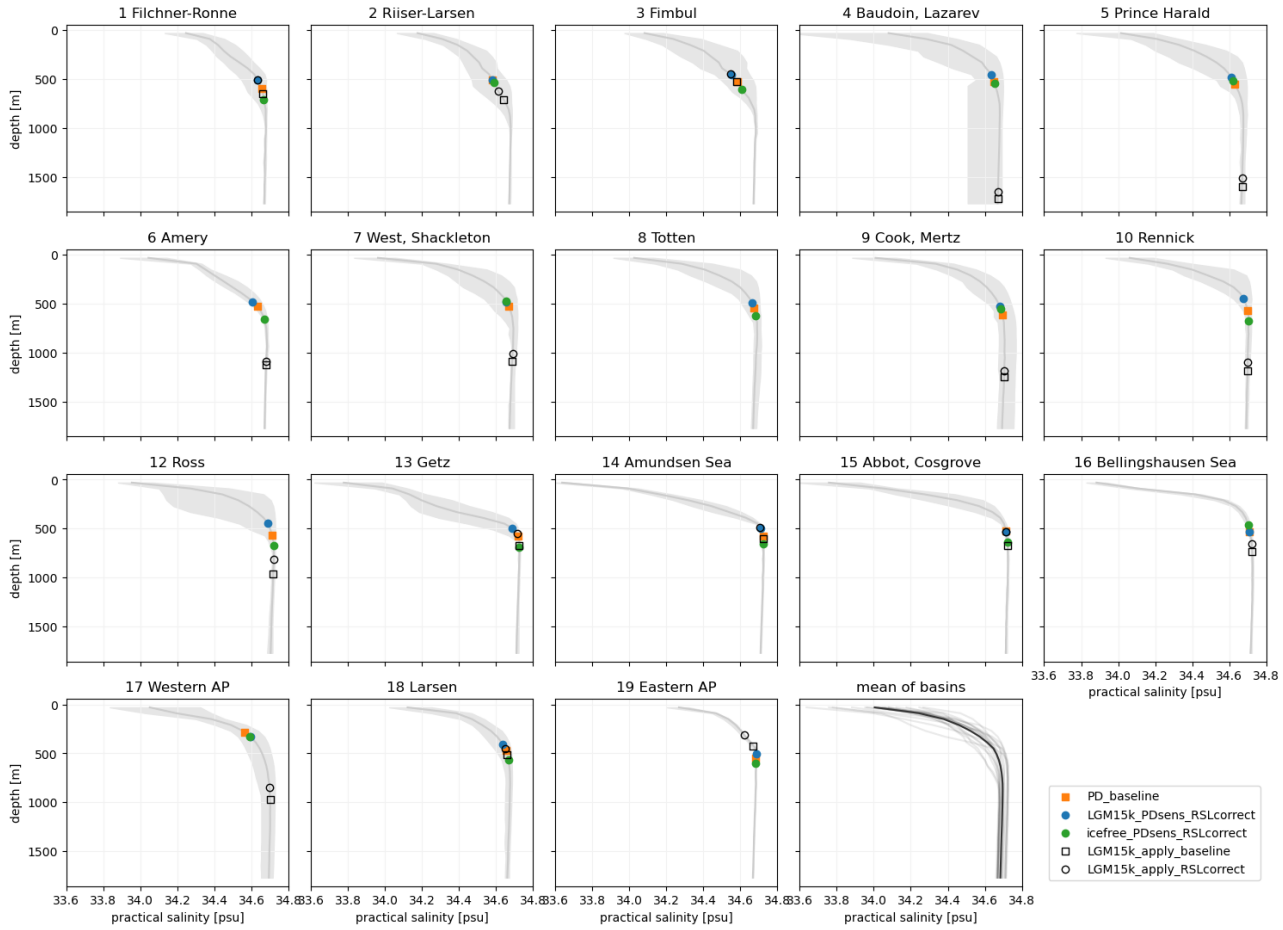

Figure S2. Vertical salinity profiles at continental-shelf break mask Same as Fig. S1, but showing practical salinity profiles instead of temperature. psu=practical salinity unit.

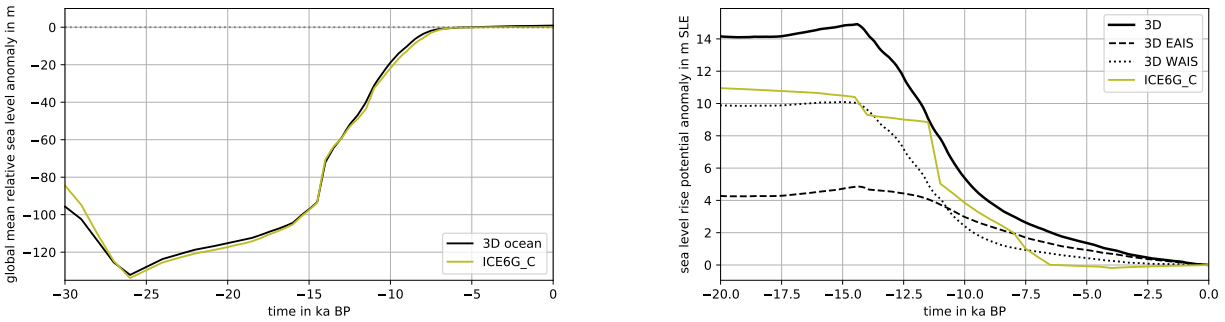

Figure S3. Global mean sea level (left) and Antarctic volume above floatation in units of sea-level rise potential (right). The global Last Glacial Maximum has been reached at ca. 26 ka BP (left), but Antarctica's LGM was at around 14.5 ka BP in our simulations (see Bentley et al. (2014) for a discussion about *Local Last Glacial Maxima*). The ICE6G_C dataset (olive color; Stuhne and Peltier, 2015) is included for comparison to the coupled ice sheet-GIA model results from PISM-VILMA (black lines).

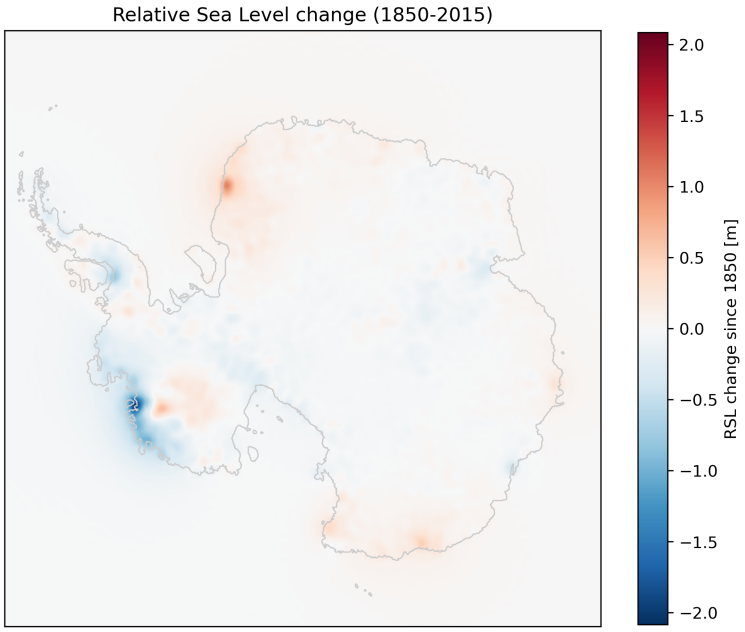

Figure S4. Relative Sea Level changes for ISMIP6 historic period. The plot shows the relative sea level change as computed by PISM–VILMA for the historic period (1850–2015) of the ISMIP6 climate forcing, see Section 2.1.2 for details. The ice-sheet grounding line at year 2015 is shown with gray contour line.

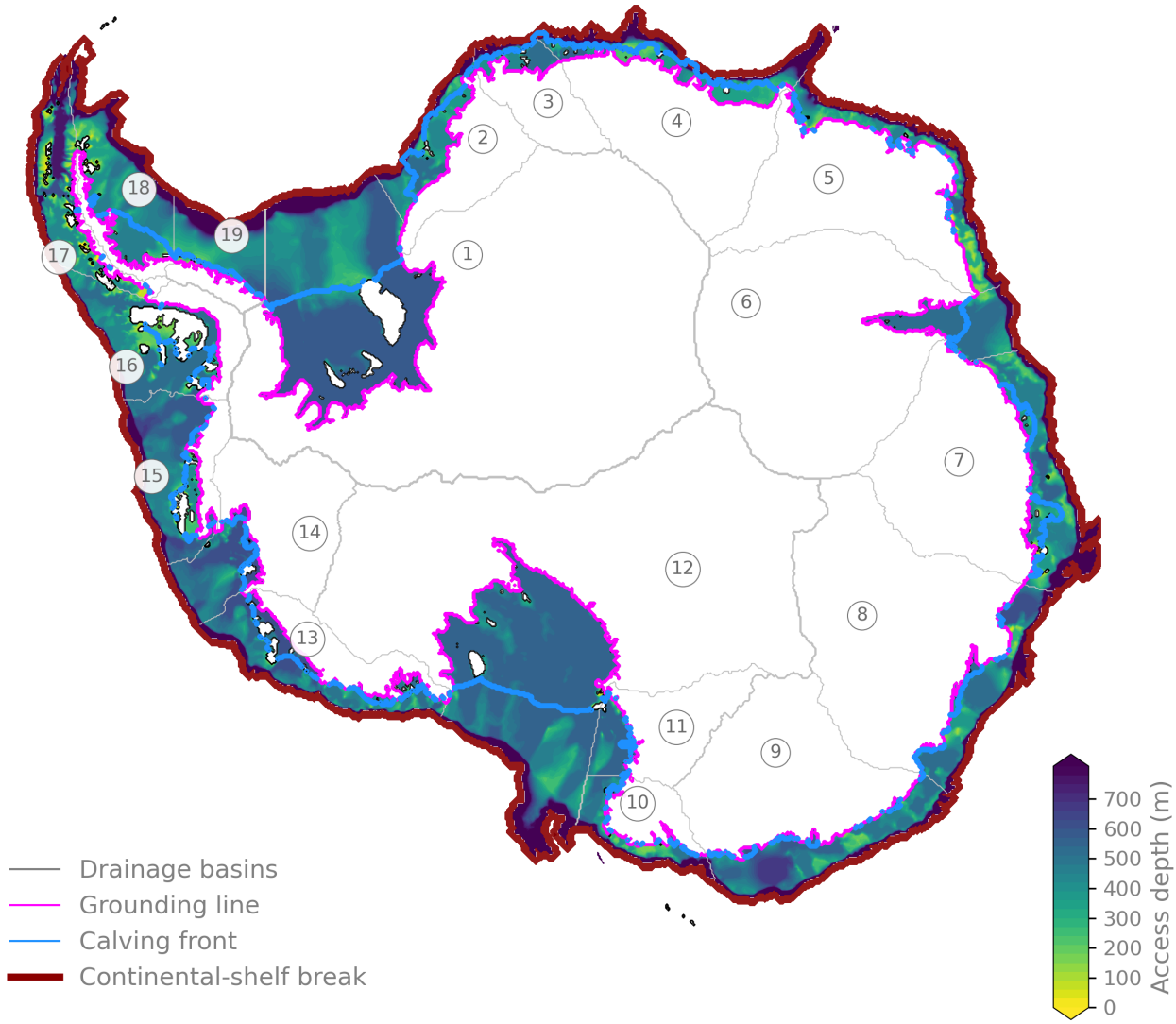

Figure S5. Access depth map d_m(present-day). Adapted from Figure 2, Nicola et al. (2023, preprint). Grey lines and corresponding numbers show ice sheet basins.

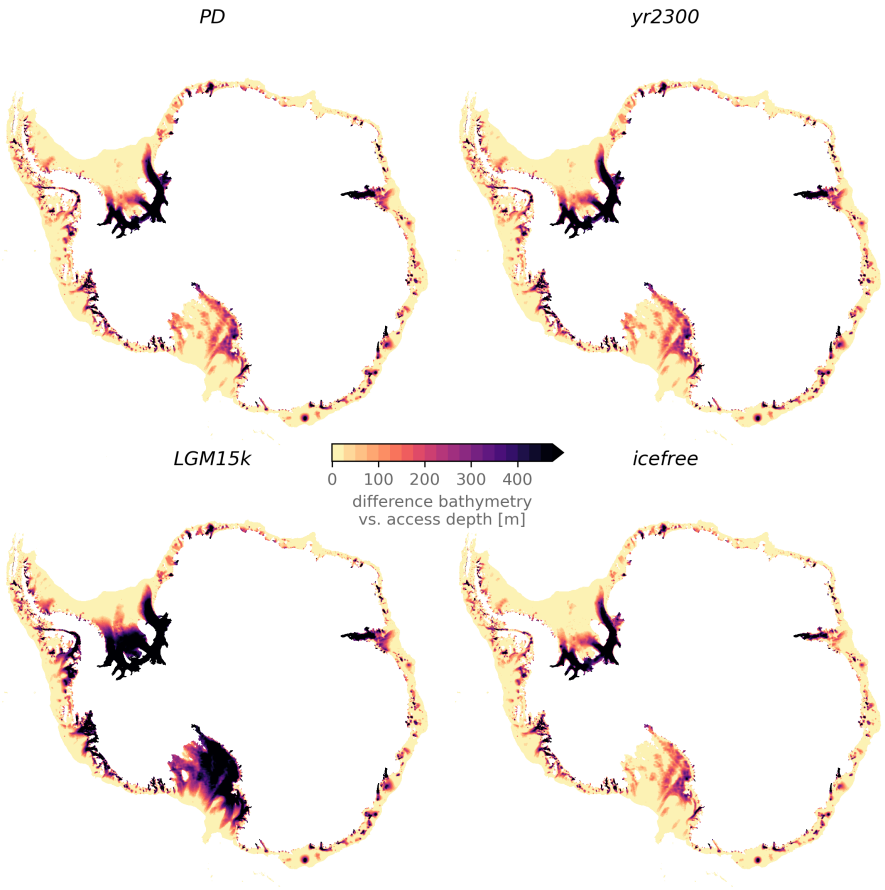

Figure S6. Regions of the Antarctic continental shelf shielded by topographic features for different RSL configurations. Color shading indicates the difference between the computed access depth maps $d_m(c)$ over the continental shelf and in the ice-shelf cavities for different RSL configurations c, compared to respective bathymetry data $t(c)$. The ice mask used here represents present-day (PD).

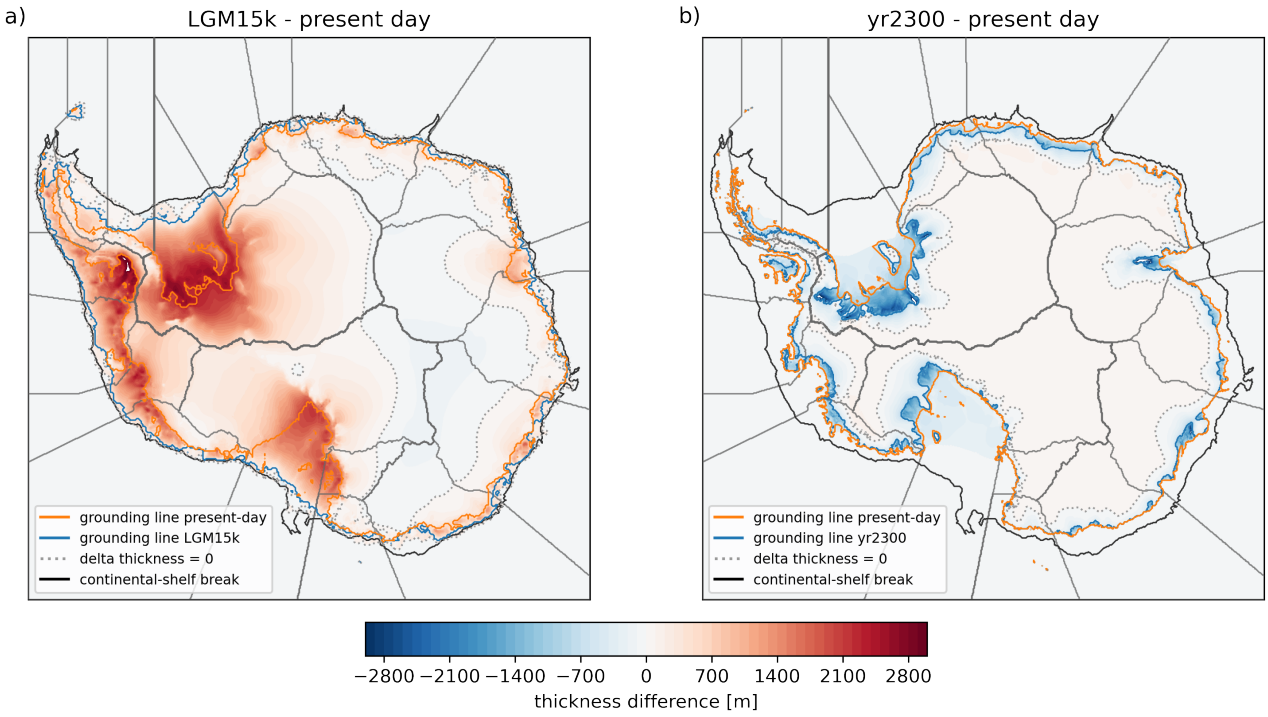

Figure S7. Ice-sheet thickness differences between a) LGM15k and b) yr2300 and present-day. Ice-sheet thickness differences are shown for states from where the respective RSL configurations have been derived from (see Section 2.1.2 for details). Grounding lines are depicted in orange for *present-day* and in blue for the respective sea-level configuration. The continental-shelf break ($z = 1800\,\mathrm{m}$ depth) is marked with a black contour line. Change between positive and negative thickness anomaly is highlighted with a dotted grey line.

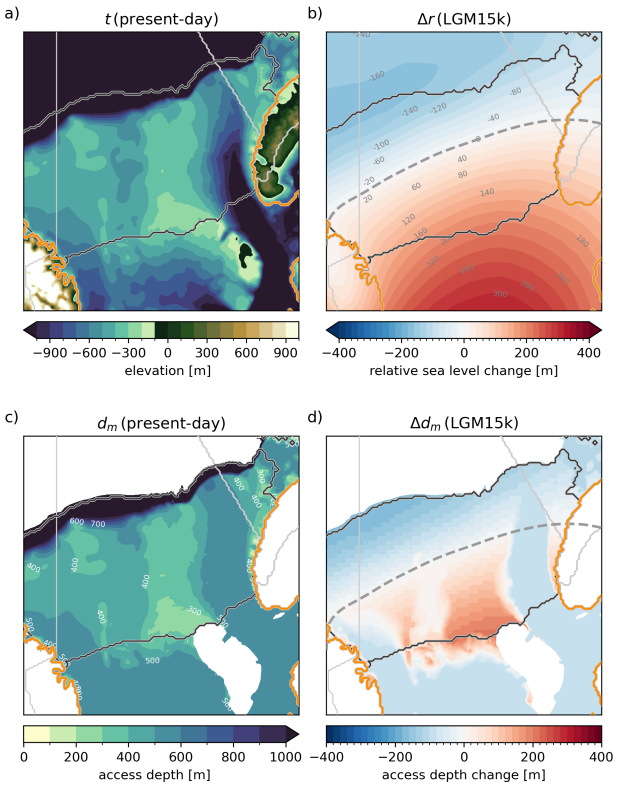

Figure S8. Influence of relative sea-level change on access depths in the Filchner-Ronne basin ($b = 1$) for the *LGM15k* RSL configuration. Upper row shows present-day topography t_{pd} (a) and the change in relative sea level Δr in the *LGM15k* configuration (b), which are both close-up views of Fig. 2. Lower panels show the derived access depth map d_m for present-day bathymetry (c) and the corresponding change Δd_m for *LGM15k* (d). Present-day grounding line is shown in orange and the continental shelf area (excluding floating ice) is marked with black contour lines. The zero contour line of RSL changes is marked as a grey dashed line in panels b) and d).

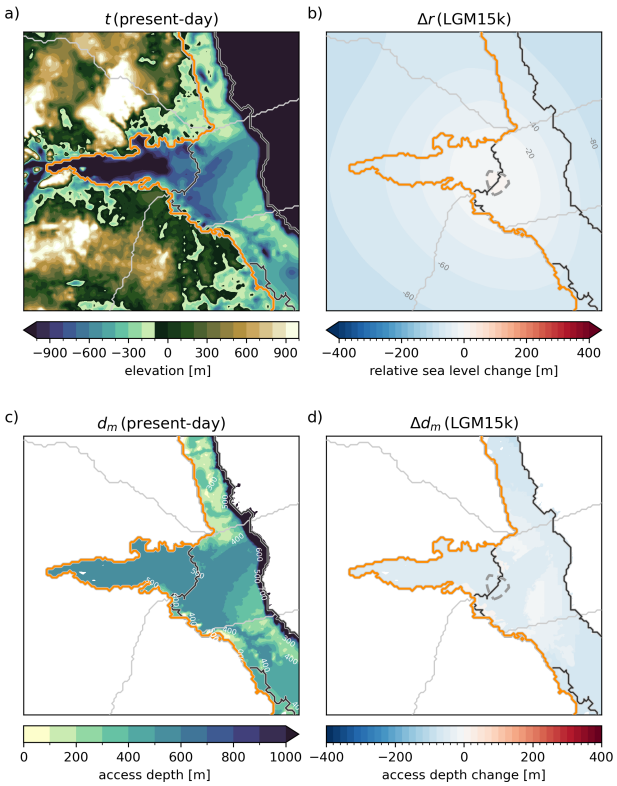

Figure S9. Influence of relative sea-level change on access depths in the Amery basin ($b = 6$) for the *LGM15k* RSL configuration. Upper row shows present-day topography t_{pd} (a) and the change in relative sea level Δr in the *LGM15k* configuration (b), which are both close-up views of Fig. 2. Lower panels show the derived access depth map d_m for present-day bathymetry (c) and the corresponding change Δd_m for *LGM15k* (d). Present-day grounding line is shown in orange and the continental shelf area (excluding floating ice) is marked with black contour lines. The zero contour line of RSL changes is marked as a grey dashed line in panels b) and d).

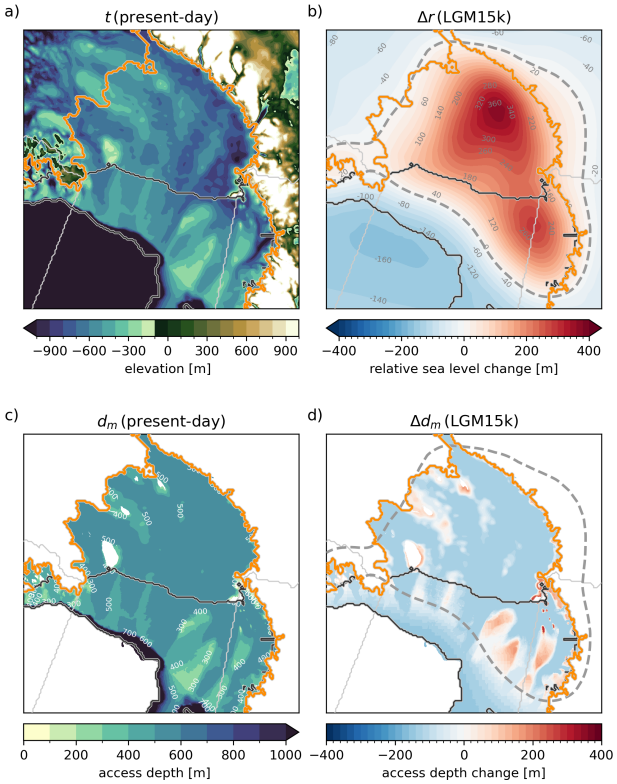

Figure S10. Influence of relative sea-level change on access depths in the Ross basin ($b = 12$) for the *LGM15k* RSL configuration. Upper row shows present-day topography t_{pd} (a) and the change in relative sea level Δr in the *LGM15k* configuration (b), which are both close-up views of Fig. 2. Lower panels show the derived access depth map d_m for present-day bathymetry (c) and the corresponding change Δd_m for *LGM15k* (d). Present-day grounding line is shown in orange and the continental shelf area (excluding floating ice) is marked with black contour lines. The zero contour line of RSL changes is marked as a grey dashed line in panels b) and d).

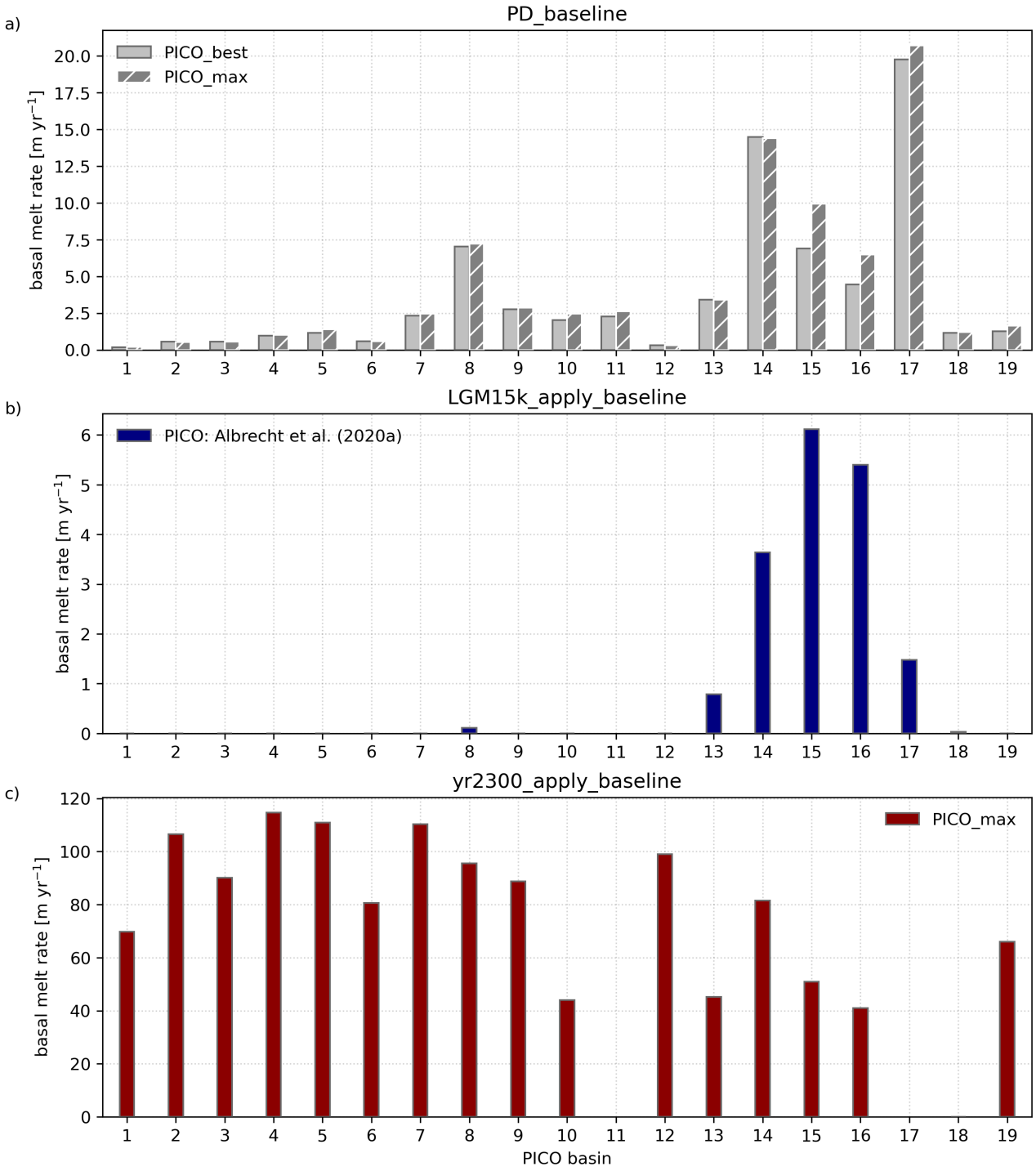

Figure S11. Basal melt rates for baseline experiments. LGM15k_apply_baseline and yr2300_apply_baseline use ice sheet geometry and ocean forcing according the corresponding RSL configuration time slice (see Sec. 2.1.2 for details), but present-day bedrock topography. The used PICO parameters are:
PICO_best=$\{C = 2.0\,\mathrm{Sv\,m^3\,kg^{-1}}, \gamma_T^* = 5 \times 10^{-5}\,\mathrm{m\,s^{-1}}\}$ (default in PD_baseline),
PICO_max=$\{C = 3.0\,\mathrm{Sv\,m^3\,kg^{-1}}, \gamma_T^* = 7 \times 10^{-5}\,\mathrm{m\,s^{-1}}\}$,
Albrecht_2020=$\{C = 0.8\,\mathrm{Sv\,m^3\,kg^{-1}}, \gamma_T^* = 1 \times 10^{-5}\,\mathrm{m\,s^{-1}}\}$.

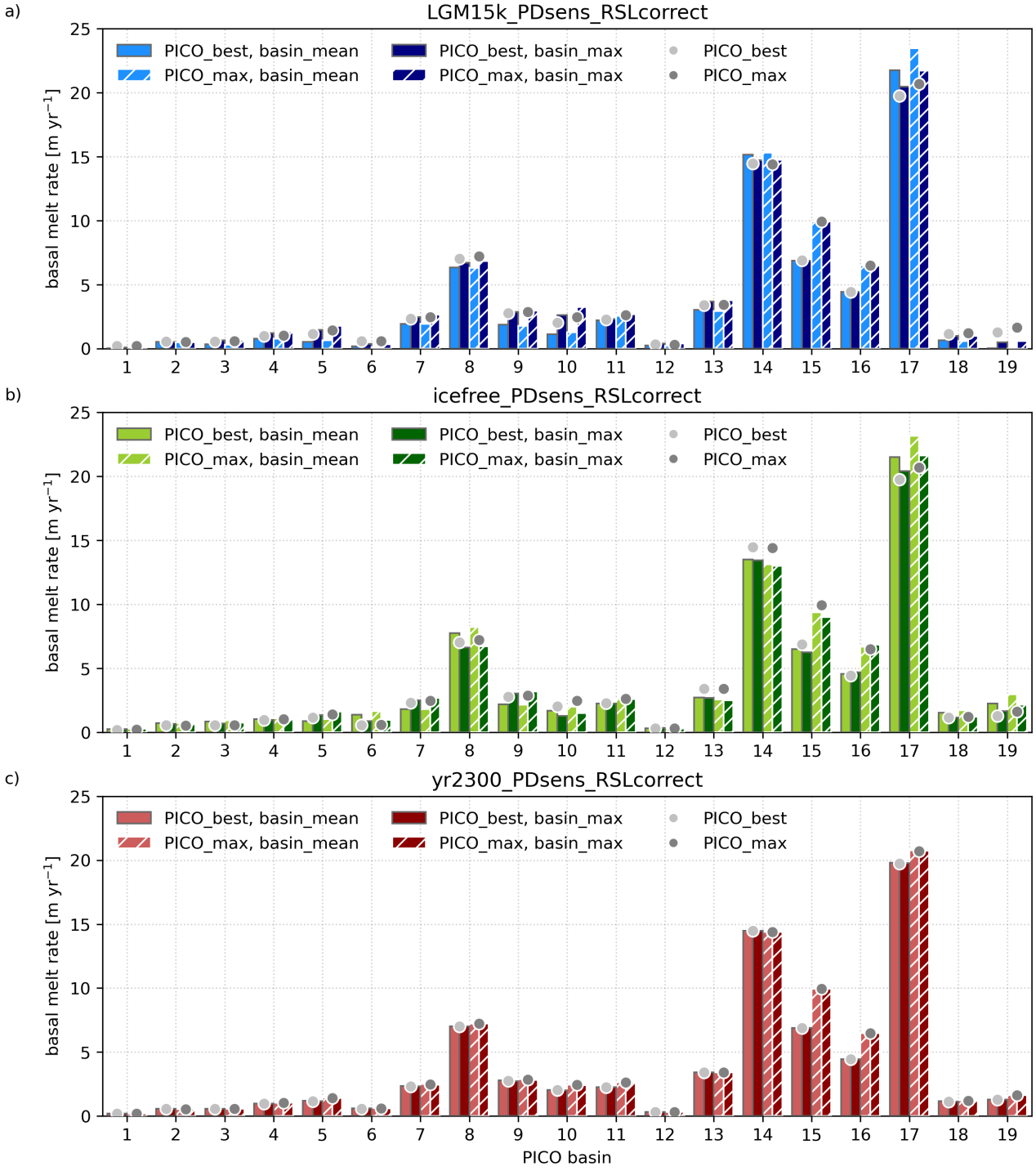

Figure S12. Melt rate sensitivity to different PICO parameters and basin reduce method for present-day sensitivity experiments. Variations in the basin reduce method are 'basin_mean' (using $\Delta T_{\mathrm{csb,mean}}$; default) and 'basin_max' ($\Delta T_{\mathrm{csb,max}}$). Grey dots correspond to present-day basline melt rates (PD_baseline), similarly as plotted in Fig. S11a.

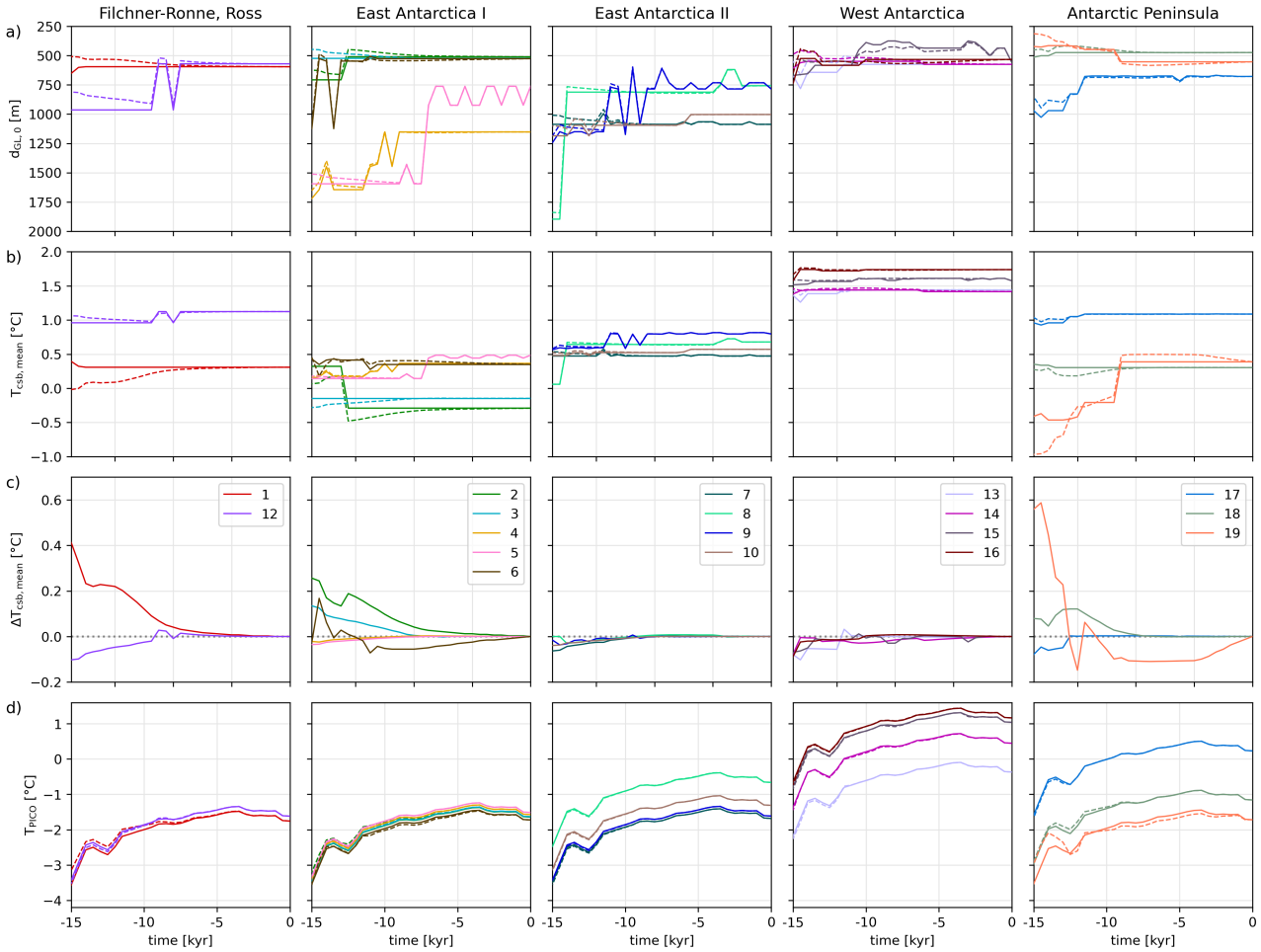

Figure S13. Deglaciation temperature corrections. Transient evolution of access depths $d_{\mathrm{GL},0}$ (a), continental-shelf break temperatures $T_{\mathrm{csb,mean}}$ (b) and their anomalies $\Delta T_{\mathrm{csb,mean}}$ (c) and resulting PICO input temperatures T_{PICO} (d) are shown for all basins. Legend for basin numbers is shown in (c). Dashed lines represent deglac_apply_RSLcorrect and solid lines deglac_apply_baseline in (a), (b) and (d).

References

Albrecht, T., Winkelmann, R., and Levermann, A.: Glacial-cycle simulations of the Antarctic Ice Sheet with the Parallel Ice Sheet Model (PISM) – Part 2: Parameter ensemble analysis, The Cryosphere, 14, 633–656, https://doi.org/10.5194/tc-14-633-2020, 2020.

Bentley, M. J., Cofaigh, C. Ó., Anderson, J. B., Conway, H., Davies, B., Graham, A. G., Hillenbrand, C.-D., Hodgson, D. A., Jamieson, S. S., Larter, R. D., Mackintosh, A., Smith, J. A., Verleyen, E., Ackert, R. P., Bart, P. J., Berg, S., Brunstein, D., Canals, M., Colhoun, E. A., Crosta, X., Dickens, W. A., Domack, E., Dowdeswell, J. A., Dunbar, R., Ehrmann, W., Evans, J., Favier, V., Fink, D., Fogwill, C. J., Glasser, N. F., Gohl, K., Golledge, N. R., Goodwin, I., Gore, D. B., Greenwood, S. L., Hall, B. L., Hall, K., Hedding, D. W., Hein, A. S., Hocking, E. P., Jakobsson, M., Johnson, J. S., Jomelli, V., Jones, R. S., Klages, J. P., Kristoffersen, Y., Kuhn, G., Leventer, A., Licht, K., Lilly, K., Lindow, J., Livingstone, S. J., Massé, G., McGlone, M. S., McKay, R. M., Melles, M., Miura, H., Mulvaney, R., Nel, W., Nitsche, F. O., O'Brien, P. E., Post, A. L., Roberts, S. J., Saunders, K. M., Selkirk, P. M., Simms, A. R., Spiegel, C., Stolldorf, T. D., Sugden, D. E., van der Putten, N., van Ommen, T., Verfaillie, D., Vyverman, W., Wagner, B., White, D. A., Witus, A. E., and Zwartz, D.: A community-based geological reconstruction of Antarctic Ice Sheet deglaciation since the Last Glacial Maximum, Quaternary Science Reviews, 100, 1–9, https://doi.org/10.1016/j.quascirev.2014.06.025, 2014.

Jourdain, N. C., Asay-Davis, X., Hattermann, T., Straneo, F., Seroussi, H., Little, C. M., and Nowicki, S.: A protocol for calculating basal melt rates in the ISMIP6 Antarctic ice sheet projections, The Cryosphere, 14, 3111–3134, https://doi.org/10.5194/tc-14-3111-2020, 2020.

Nicola, L., Reese, R., Kreuzer, M., Albrecht, T., and Winkelmann, R.: Oceanic gateways to Antarctic grounding lines – Impact of critical access depths on sub-shelf melt, EGUsphere, 2023, 1–30, https://doi.org/10.5194/egusphere-2023-2583, 2023.

Stuhne, G. R. and Peltier, W. R.: Reconciling the ICE-6G_C reconstruction of glacial chronology with ice sheet dynamics: The cases of Greenland and Antarctica, Journal of Geophysical Research: Earth Surface, 120, 1841–1865, https://doi.org/10.1002/2015jf003580, 2015.